LAWRENCE
LIVERMORE
NATIONAL
LABORATORY

UCRL-JRNL-224213

Laboratory measurements of high-n iron L-shell x-ray lines

H. Chen, M. F. Gu, E. Behar, G. V. Brown, S. M. Kahn, P. Beiersdorfer

September 6, 2006

Astrophysical Journal Suppliment Seriers

Updated October 14, 2003

Laboratory measurements of high-n iron L-shell x-ray lines

H. Chen[⋆], M. F. Gu[†], E. Behar[§], G.V. Brown[⋆], S. M. Kahn[†] and P. Beiersdorfer[⋆]

[⋆] *High Temperature and Astrophysics Division, Lawrence Livermore National Laboratory, Livermore, CA 94551*

[†] *Physics Department, Stanford University, CA 94305*

[§] *Physics Department, Technion Israel Institute of Technology, Haifa 32000, Israel*

ABSTRACT

We present a comprehensive wavelength survey of Fe L-shell X-ray lines between 7 and 11 Å measured using flat crystal spectrometers and the EBIT-I and EBIT-II electron beam ion traps at the Lawrence Livermore National Laboratory. This survey includes all significant emission lines produced by over 200 $n \rightarrow 2$ transitions in Fe XIX – XXIV, with n=4–10. The identification and assignment of transitions are made with the help of detailed theoretical modeling using the Flexible Atomic Code (FAC).

Subject headings: atomic data — line: identification — Sun: X-rays, gammma rays —X-rays: general

1. Introduction

Accurate atomic data are crucial for the modeling of observed line intensities and for deriving the plasma conditions critical for the interpretation of astrophysical observations (Kahn & Liedahl 1990; Paerels & Kahn 2003). The atomic data of iron are particularly important for interpreting virtually all types of observations since iron is the most abundant high-Z element and radiates profusely in many spectral bands. Specifically, the line-rich emission from the iron L-shell transitions has been one of the primary diagnostic tools of the high-resolution grating spectrometers on the $XMM-Newton$ and $Chandra$ X-ray observatories. The detailed spectra obtained by these missions provide constraints on the complex physical processes occurring in hot, cosmic plasmas and make possible X-ray line diagnostics for a wide range of astrophysical sources. Such applications in turn rely heavily upon the accuracy of the atomic data on which models and data interpretation are based. To address the need for a complete, accurate set of atomic data, our laboratory

X-ray astrophysics program has utilized the electron beam ion traps EBIT-I and EBIT-II at the University of California Lawrence Livermore National Laboratory (Beiersdorfer 2003). Earlier, we have measured a complete set of Fe L-shell $n = 3 \rightarrow 2$ emission lines, which fall into the wavelength range from 10.6 Å up to 18 Å (Brown et al. 1998, 2002). As an extension of that work, we now present a comprehensive survey of the Fe L-shell X-ray lines corresponding to $n \rightarrow 2$ (with $n > 3$) transitions, which fall into the wavelength range from 11 Å down to 6 Å. Although the line intensities are generally weaker compared to the $n = 3 \rightarrow 2$ emission, these high $n \rightarrow 2$ Fe lines contribute, in some case substantially, to the "background" and blend with other lines observed in many astrophysical sources, such as the lines of K-shell Mg and Si, which also fall in the wavelength band. Moreover, as has been discussed previously (Mason & Storey 1980; Fawcett et al. 1987; Wargelin et al. 1998; Mauche et al. 2003; Chen et al. 2004, 2006), some of the Fe lines are electron density sensitive, and therefore, can be used as density diagnostics.

In the following we present our measurement and identification of the high $n \rightarrow 2$ transition lines. The line identification was made through detailed theoretical modeling using the Flexible Atomic Code (Gu 2003) described in Section 3. As we discuss in Section 4, we have identified 168 features, which we associated with over 200 transitions. The present line list thus provides a comprehensive data set for use in spectral modeling codes such as APEC (Smith et al. 2001) and CHIATI (Landi et al. 2006) as well as a benchmark of *abinitio* codes such as HULLAC (Bar-Shalom et al. 2001) and FAC (Gu 2003).

2. Emission line measurements

Our experiments were carried out on the EBIT-I (Levine et al. 1988) and EBIT-II electron beam ion traps using two flat-crystal spectrometers. Details of the spectrometers can be found in Beiersdorfer & Wargelin (1994) and Brown et al. (1999). The iron spectra were taken at four settings utilizing two types of crystals to cover the wavelength range from 7 to 11 Å. The wavelength range of 7 – 9 Å was covered in three settings using a 50 mm × 25 mm × 25 mm ammonium dihydrogen phosphate (ADP) crystal, while the forth setting used a 50 mm × 25 mm × 25 mm thallium hydrogen phthalate (TlAP) crystal for the wavelength range of 9 – 11 Å. Neighboring settings have wavelength overlap of 0.1 – 0.2 Å. For each setting, a total of 2 – 9 spectra were taken at different electron beam energies (1.5–3.0 keV). The beam energies were selected to maximize the population of particular charge states in a single spectrum.

Two injection methods were used to introduce iron into the trap. One employed a metal vapor vacuum arc source (MeVVA) (Brown et al. 1986) and the other a gas injector. The

first method utilizes element iron, while the other an iron compound, iron pentacarbonyl ($Fe(CO)_5$). The MeVVA injection was used for the three lower wavelength settings, and the gas injection was used for the fourth, longest wavelength setting. In both cases, the injected ions were trapped for times between 4 and 5 seconds and then expelled before a new cycle of injection began. The ions are cycled in this fashion to avoid contamination of the trap by heavy elements. Indeed, there was no contamination from high-Z ions in the measurements. To check for any possible background emission, we took spectra at the same operation conditions except without iron injection. As expected and shown in Section 4, the MeVVA injection resulted in a higher average ion charge state than that from the gas injection. This is because in the case of the MeVVA injection, the ions are successively ionized until they reach a charge defined by the electron beam energy. In the case of gas injection, $Fe(CO)_5$ continuously flows into the trap and thus replenishes the low charge states continuously. Thus the later method results in an equilibrium consisting of broader range of charge states than in the case of the MeVVA injection.

To calibrate the wavelength scale, we used a combination of Li-like and He-like lines of Mg^{9+} and Mg^{10+}, earlier measurements of several high-n transitions of Fe XXI – XXIV observed in the Princeton Large Torus (PLT) tokamak (Wargelin et al. 1998), and the measurement of the $3 \rightarrow 2$ transitions of Fe^{22+} near 11 Å by Brown et al. (2002). The calibration lines are listed in Table 1. The calibration lines were analyzed in the same way as described by Brown et al. (2002). The total calibration uncertainties are estimated to be 2 mÅ for the 7 – 9 Å range covered by the ADP crystal. For the 9 – 11 Å range covered by the TlAP crystal, the uncertainty is 4 mÅ due to the uncertainty of the calibration lines and the lower resolving power of the spectrometer. The statistical uncertainties are below 1 mÅ for most of the strong lines. The total error quoted for the measured wavelength is the quadrature addition of each individual error.

3. Data Analysis and Modeling Using the FAC code

In order to identify the multitude of Fe lines, we constructed theoretical models with mono-energetic electron excitation conditions. In our model, collisional excitation from the $n = 2$ configurations of each charge state to configurations with $n \leq 12$ and the subsequent radiative cascades were included. The atomic data needed, including level energies, collision strengths, and radiative transition rates, were calculated with the Flexible Atomic Code (FAC) described by Gu (2003). The spectra were computed at an electron density of 10^{11} cm^{-3}, which is appropriate for the experimental conditions of the present work, and corresponds to the coronal density limit for most Fe L-shell ions. The theoretical spectra for

individual charge states were properly weighted by the fractional ion abundance to fit the measured data, with the weighting coefficients treated as free parameters. The relative spectrometer response was estimated by taking into account the absorption in the filters between the spectrometer and the electron beam ion trap, the gas absorption in the gas proportional counters, which were filled with P-10 (10% CH_4 and 90% Ar) gas at 1 atmosphere and a depth of 0.9 cm, as well as the relative reflectivity of each crystal. We used Voigt line profiles in the spectral fit with fixed widths and damping parameters for each spectrometer setting derived by fitting isolated lines. Overall good agreements between the model spectra and data are obtained for all spectral settings and electron energies.

An example of our modeling spectra is shown in Fig. 1. The figure displays a spectrum taken at an electron beam energy of 1.95 keV and in the spectral region of 8–9 Å. C-like, B-like, and Be-like ions are the major contributors to this spectrum. The best-fit relative abundances of these ions are determined to be 0.18, 0.33, and 0.48, respectively. Contributions from individual charge states are shown in Figure 1 to assist assigning lines to different ions.

With the aid of our modeling, we could identify the strongest features in each observed spectrum. We then determined the wavelengths and intensities of the associated transitions by fitting multi-Voigt components to individual features in the local spectral regions. When the same transitions were measured in multiple spectra, instead of averaging over all wavelengths and uncertainties, we chose the measurement from the spectrum with the highest signal-to-noise ratio and least amount of blending as the final result. The differences of wavelengths measured in different spectral are typically below the calibration errors, and for most lines, the statistical uncertainty obtained in a single measurement is less than the calibration error as well. Therefore averaging would not improve the accuracy of the measurements further. The measured intensities were then normalized to the strongest line for each charge state. The intensities obtained in different spectral settings were related to each other through overlapping regions. Theoretical transitions contributing more than 20% to a given peaks were assigned to that feature.

4. Results and Discussions

Our results are summarized in Tables 2–7, and illustrated in Figures 2–7. We continue the labeling convention and numerical consequence started by Brown et al. (2002). For comparison, the tables also include the results of the solar flare spectra reported by McKenzie et al. (1985) and Fawcett et al. (1987), and the measurements by Wargelin et al. (1998) on PLT tokamak plasma.

4.1. F-like Fe XVIII and O-like Fe XIX lines

We observed two F-like and five O-like Fe features, as shown in Fig. 2. The corresponding ten atomic transitions associated with these seven features are listed in Table 2. These lines are $4d$ – $2p$ (Fe XIX) and $5d$ – $2p$ (Fe XVIII) transitions. The strongest line in the spectrum is O32 line at 10.818 Å. We identify the associated transition to be $2p^2_{3/2}(J = 2)$ to $2p_{3/2}4d_{3/2}(J = 3)$. Two lines, O36 and F38, are blended with N-like lines.

4.2. N-like Fe XX lines

22 N-like Fe XX features were measured in two settings, as shown in Fig. 3(a) and (b). These were identified to be associated with transitions from levels with principal quantum number $n \leq 7$, as listed in Table 3. The majority of these features are associated with multiple atomic transitions, as these transitions make a comparable contribution to the intensity of a given line. Two transitions are the dominant contributors to the strongest line N46 at 10.004 Å: $2p_{3/2}(J = \frac{3}{2})$ to $2p_{1/2}2p_{3/2}4d_{3/2}(J = \frac{3}{2})$ and $2p_{3/2}(J = \frac{3}{2})$ to $2p_{1/2}2p_{3/2}4d_{3/2}(J = \frac{5}{2})$.

4.3. C-like Fe XXI lines

In the C-like Fe XXI spectrum, we observed 44 features in three measurement settings, as illustrated in Fig. 4(a), (b) and (c). The associated atomic transitions (n=4–10 to 2) are listed in Table 4. Most of the lines were associated with single atomic transition. The measurements generally agree with the theoretical wavelengths within a few mÅ except for a couple of lines (C34 and C33) where the difference is slightly bigger (8–9 mÅ).

4.4. B-like Fe XXII lines

We observed 51 B-like Fe XXII lines in four measurement settings, as illustrated in Fig. 5(a), (b), (c), and (d). The corresponding atomic transitions (n=4–10 to 2) are listed in Table 5. Nearly half of the lines are attributed to multiple transitions. The strongest line at 8.977 Å is identified with the $2p_{1/2}(J = \frac{1}{2})$ to $4d_{3/2}(J = \frac{3}{2})$ transition. The identifications for B63 and B66 lines are tentative for the agreement between the model and measurement is poor. Although the theoretical wavelengths match the observed features, but the modeled intensities are much less (up to 50%) than that were measured. The reason for this disagreement is not clear although one may speculate it to be the cross sections used in the model,

or other reasons unknown to us.

An important property of N-like, O-like, C-like and B-like lines is their potential to serve as electron density diagnostics. The density sensitivity of these lines is based on the fine structure splitting of the ground configuration. For example, for B-like Fe ions, the $2p$ ground configuration splits into $2p_{3/2}(J = \frac{3}{2})$ and $2p_{1/2}(J = \frac{1}{2})$. At low densities, the true ground level, $1s^2 2s^2 2p_{1/2}\ ^2P_{1/2}$, is almost exclusively populated, whereas the population of the upper (metastable) level of the ground term, $1s^2 2s^2 2p_{3/2}\ ^2P_{3/2}$, is insignificant. At the high density limit, the population ratio of the $2p_{1/2}$ and $2p_{3/2}$ levels reflects the local thermodynamic equilibrium and thus approaches the statistical ratio 1:2. In between these limits, the population ratio reflects the density of the plasma. A few density sensitive features of the L-shell spectra of C-like and B-like ions have been discussed previously by Mason & Storey (1980); Fawcett et al. (1987); Wargelin et al. (1998); Mauche et al. (2003); Chen et al. (2004) and Chen et al. (2006).

4.5. Be-like Fe XXIII lines

We observed 28 Be-like Fe XXII lines in four measurement settings, as shown in Fig. 6(a), (b), (c), and (d). The corresponding atomic transitions (n=3–9 to 2) are listed in Table 6. Five lines (Be16, Be 17, Be21, Be30 and Be32) are blended with either B-like or C-like lines. The identification of 3 lines (Be33, Be34 and Be36) is tentative, again for the poor agreement between modeled and measured line intensities.

4.6. Li-like Fe XXIV lines

In total, 16 Li-like Fe XXIV lines were measured in four measurement settings, as displayed in Fig. 7(a), (b), (c) and (d). The corresponding atomic transitions (n=3–6 to 2) are listed in Table 7. Many of these high n to 2 Li-like Fe lines have been observed before in solar flares (McKenzie et al. 1985; Fawcett et al. 1987), laser plasmas (Boiko, Faenov & Pikuz 1978) and tokamak plasmas (Wargelin et al. 1998). We identified the majority of the lines with a single trantions. The only exception is the line labeled Li17. Moreover, line Li8 is blended with line Be21. We confirmed the identification for the line at 7.461 Å to be a transition from $2p_{3/2}(J = \frac{3}{2})$ to $5s_{1/2}(J = \frac{1}{2})$. This line was tentatively identified by Wargelin et al. (1998).

5. Summary

We have presented results from measurements on the EBIT-I and EBIT-II machines of highly ionized Fe L-shell lines between approximately 7 and 11 Å. We have identified almost every line through theoretical modeling using FAC. These lines are from high-n (n=4, 5, up to 10) to 2 transitions. The combination of the present measurements with our previous catalogue of the Fe L-shell 3 $\rightarrow$ 2 transitions provides the most extensive and accurate laboratory X-ray line list for Fe L-shell ions to date.

This work was performed under the auspices of the U.S. Department of Energy by the University of California Lawrence Livermore National Laboratory under contract No. W-7405-Eng-48 and supported by NASA Astronomy and Physics Research and Analysis grants to LLNL and Stanford University.

REFERENCES

Bar-Shalom, A., Klapisch, M., & Oreg, J. 2001, J. Quant. Spec. Radiat. Transf., 71, 169

Beiersdorfer,P. & Wargelin, B. J., 1994, Rev. Sci. Instrum., 65, 13

Beiersdorfer, P., 2003, Annu. Rev. Astron. Astrophys., 41, 343

Boiko, V. A., Faenov, A. Ya., & Pikuz, S. A., 1978, J. Quant. Spectrosc. Radiat. Transfer, 19, 11

Brown, I. G., Galvin, J. E., MacGill, R. A., & Wright, R. T., 1986, Appl. Phys., 49, 1019

Brown, G. V., Beiersdorfer, P., Liedahl, D. A., Widmann, K. & Kahn, S. M. 1998, ApJ, 502, 1015

Brown, G. V., Beiersdorfer, P., & Widmann, K., 1999, Rev. Sci. Instrum., 70, 280

Brown, G. V., Beiersdorfer, P., Liedahl, D. A., Widmann, K., Kahn, S. M. & Clothiaux, E. J., 2002, ApJS, 140, 589

Chen, H., Beiersdorfer, P., Heeter, L. A., Liedahl, D. A., Naranjo-Rivera, K. L., Träbert, E., Gu, M. F. & Lepson, J. K. 2004, ApJ, 611,598

Chen, H., Gu M. F., Beiersdprfer P., Boyce K. R., Brown G. V., Kelly R. L., Kilbourne C. A., Porter F. S., Kahn S. M. & Scofield J., 2006, ApJ, 646, 653

Fawcett, B. C., Jordan, C., Lemen, J. R., & Phillips, K. J. H. 1987, Mon. Not. R. astr. Soc., 225, 1013

Gu, M. F.,2003, ApJ, 582, 1241

Kahn, S. M., & Liedahl, D. A., 1990, in Iron Line Diagnostics in X-ray Sources, edited by A. Treves, G. C. Perola & L. Stella, Springer-Verlag, p3

Landi, E., Del Zanna, G., Young, P. R., Dere, K. P., Mason, H. E., Landini, M., ApJS, 162, 261

Levine, M. A., Marrs, R. E., Henderson, J. R., Knapp, D. A., & Schneider, M. B., 1988, Physics Scripta, T22, 157

Mason, H. E. & Storey, P. J., 1980, MNRAS, 191, 631

Mauche, C. W., Liedahl, D. A., & Fournier, K. B. 2003, ApJ, 588, L101

McKenzie, D. L., Landecker, P. B., Feldman, U., & Doschek, G. A., 1985, ApJ, 289, 849

Smith, R. K., Brickhouse, N. S., Liedahl, D. A., Raymond, J. C., ApJ, 556, L91

Paerels, F. B. S. & Kahn, S. M., 2003, Ann. Rev. Astron. Astrophys., 41, 291

Wargelin, B. J., Beiersdorfer, P., Liedahl, D. A., Kahn, S. M., & von Goeler, S., 1998, ApJ, 496, 1031

Table 1. Wavelength calibration lines

Ion	Transition	Wavelength (Å)	References
Mg^{10+}	Kϵ	7.2247 ± 0.0003	(1)
Mg^{10+}	Kδ	7.3103 ± 0.0002	(1)
Mg^{10+}	Kγ	7.4731 ± 0.0002	(1)
Mg^{10+}	Kβ	7.8503 ± 0.0003	(1)
Mg^{10+}	w	9.1685 ± 0.0003	(1)
Mg^{10+}	xy	9.2310 ± 0.0003	(1)
Mg^{9+}	q	9.2832 ± 0.0003	(1)
Mg^{10+}	z	9.3140 ± 0.0008	(1)
Fe^{23+}	$2p^2P_{3/2} - 4d^2D_{5/2}$	8.3161 ± 0.0003	(1)
Fe^{22+}	$2s2p^1P_1 - 2s4d^1D_2$	8.8149 ± 0.0004	(1)
Fe^{21+}	$2s^22p^2P_{1/2} - 2s^24d^2D_{3/2}$	8.9748 ± 0.0006	(1)
Fe^{21+}	$2s^2 - 2s_{1/2}3p_{3/2}$	10.981 ± 0.003	(2)

References. — (1) Wargelin, B. J., Beiersdorfer, P., Liedahl, D. A., Kahn, S. M., & von Goeler, S., 1998, ApJ496, 1031, and reference cited in. (2) Brown, G. V., Beiersdorfer, P., Liedahl, D. A., Widmann, K., Kahn, S. M. & Clothiaux, E. J., 2002, ApJS, 140, 589

Table 2. F-like Fe XVIII and O-like Fe XIX lines

Label	$\lambda_{\rm exp}$[a]	Iexp [b]	$\lambda_{\rm FAC}$ [c]	$I_{\rm FAC}$ [d]	Lower [e]	Upper [f]
O32	10.818(6)	100.0	10.824	72.0	$2p^2_{3/2}(J=2)$	$2p_{3/2}4d_{3/2}(J=3)$
O34	10.682(7)	30.4	10.693	21.5	$2p^2_{3/2}(J=2)$	$2p_{1/2}2p^2_{3/2}4d_{3/2}(J=3)$
O35	10.645(6)	85.1	10.642	46.3	$2p^2_{3/2}(J=2)$	$2p_{1/2}2p^2_{3/2}4d_{3/2}(J=2)$
			10.650	42.8	$2p^2_{3/2}(J=2)$	$2p_{1/2}2p^2_{3/2}4d_{3/2}(J=3)$
O36 [bl1]	10.127(6)	38.2	10.138	5.0	$2p^2_{3/2}(J=2)$	$2s_{1/2}2p^2_{3/2}4p_{3/2}(J=3)$
O37	9.850(6)	63.3	9.853	29.6	$2p^2_{3/2}(J=2)$	$2p_{3/2}5d_{5/2}(J=3)$
F37	10.537(8)	100.0	10.539	76.9	$2p^3_{3/2}(J=\frac{3}{2})$	$2p^2_{3/2}5d_{5/2}(J=\frac{5}{2})$
			10.540	37.2	$2p^3_{3/2}(J=\frac{3}{2})$	$2p^2_{3/2}5d_{5/2}(J=\frac{3}{2})$
			10.546	5.6	$2p^3_{3/2}(J=\frac{3}{2})$	$2p^2_{3/2}5d_{5/2}(J=\frac{1}{2})$
F38 [bl2]	10.452(8)	12.1	10.449	6.3	$2p^3_{3/2}(J=\frac{3}{2})$	$2p_{1/2}2p^3_{3/2}5d_{3/2}(J=\frac{5}{2})$

[a]Measured wavelength in Å. Numbers in the parentheses are the estimated uncertainties in mÅ.

[b]Measured relative intensities, normalized to 100, the strongest line for each charge state.

[c]Calculated wavelengths (in Å) using configuration interaction theory using FAC code.

[d]Calculated relative intensity.

[e]Configuration labels for the lower levels.

[f]Configuration labels for the upper levels.

[bl1]blended with line N44 (see Table 3).

[bl2]blended with line N39 (see Table 3).

Table 3. N-like Fe XX lines

Label	$\lambda_{\rm exp}$[a]	$I_{\rm exp}$ [b]	Ion [c]	$\lambda_{\rm FAC}$ [d]	$I_{\rm FAC}$ [e]	Lower [f]	Upper [g]
N39,F38	10.452(8)	12.1	N	10.454	6.5	$2s_{1/2}2p_{1/2}2p^3_{3/2}(J=\frac{3}{2})$	$2s_{1/2}2p_{3/2}4d_{5/2}(J=\frac{5}{2})$
			F	10.449	6.3	$2p^3_{3/2}(J=\frac{3}{2})$	$2p_{1/2}2p^3_{3/2}5d_{3/2}(J=\frac{5}{2})$
			N	10.453	3.4	$2s_{1/2}2p_{1/2}2p^3_{3/2}(J=\frac{3}{2})$	$2s_{1/2}2p_{3/2}4d_{5/2}(J=\frac{3}{2})$
			N	10.476	2.7	$2s_{1/2}2p^2_{3/2}(J=\frac{1}{2})$	$2s_{1/2}2p_{3/2}4d_{5/2}(J=\frac{1}{2})$
			N	10.478	2.7	$2s_{1/2}2p^2_{3/2}(J=\frac{1}{2})$	$2s_{1/2}2p_{3/2}4d_{5/2}(J=\frac{3}{2})$
N40	10.391(11)	6.1	N	10.396	1.3	$2p_{1/2}2p^2_{3/2}(J=\frac{3}{2})$	$2p_{1/2}2p_{3/2}4s_{1/2}(J=\frac{1}{2})$
			N	10.389	1.1	$2p_{1/2}2p^2_{3/2}(J=\frac{5}{2})$	$2p_{1/2}2p_{3/2}4s_{1/2}(J=\frac{3}{2})$
			N	10.401	1.0	$2p_{1/2}2p^2_{3/2}(J=\frac{5}{2})$	$2p_{1/2}2p_{3/2}4s_{1/2}(J=\frac{5}{2})$
N41	10.368(7)	16.7	N	10.379	14.4	$2s_{1/2}2p^2_{3/2}(J=\frac{5}{2})$	$2s_{1/2}2p_{3/2}4d_{3/2}(J=\frac{7}{2})$
N42	10.258(8)	13.5	N	10.265	8.1	$2p_{1/2}2p^2_{3/2}(J=\frac{3}{2})$	$4d_{5/2}(J=\frac{5}{2})$
			N	10.262	3.3	$2p_{1/2}2p^2_{3/2}(J=\frac{1}{2})$	$2p_{1/2}2p_{3/2}4d_{5/2}(J=\frac{1}{2})$
N43	10.182(8)	12.8	N	10.181	10.1	$2p_{1/2}2p^2_{3/2}(J=\frac{3}{2})$	$2p_{1/2}2p_{3/2}4d_{5/2}(J=\frac{5}{2})$
			N	10.188	4.2	$2p_{1/2}2p^2_{3/2}(J=\frac{5}{2})$	$2p_{1/2}2p_{3/2}4d_{3/2}(J=\frac{5}{2})$
N44,O36	10.127(6)	38.2	N	10.118	22.1	$2p_{3/2}(J=\frac{3}{2})$	$4d_{5/2}(J=\frac{5}{2})$
			O	10.138	5.0	$2p^2_{3/2}(J=2)$	$2s_{1/2}2p^2_{3/2}4p_{3/2}(J=3)$
N45	10.056(6)	56.3	N	10.050	30.5	$2p_{3/2}(J=\frac{3}{2})$	$2p_{1/2}2p_{3/2}4d_{3/2}(J=\frac{5}{2})$
			N	10.056	6.4	$2p_{3/2}(J=\frac{3}{2})$	$2p_{1/2}2p_{3/2}4d_{3/2}(J=\frac{3}{2})$
N46	10.004(5)	100.0	N	10.000	48.6	$2p_{3/2}(J=\frac{3}{2})$	$2p_{1/2}2p_{3/2}4d_{3/2}(J=\frac{3}{2})$
			N	10.005	29.1	$2p_{3/2}(J=\frac{3}{2})$	$2p_{1/2}2p_{3/2}4d_{3/2}(J=\frac{5}{2})$
	9.997 [i]						
	10.000 [j]						
N47	9.713(6)	42.1	N	9.723	12.6	$2p_{3/2}(J=\frac{3}{2})$	$2s_{1/2}2p_{3/2}4p_{3/2}(J=\frac{5}{2})$
N48	9.072(2)	35.6	N	9.079	16.3	$2p_{3/2}(J=\frac{3}{2})$	$2p_{1/2}2p_{3/2}5d_{3/2}(J=\frac{3}{2})$
			N	9.078	10.4	$2p_{3/2}(J=\frac{3}{2})$	$2p_{1/2}2p_{3/2}5d_{3/2}(J=\frac{1}{2})$
			N	9.081	8.6	$2p_{3/2}(J=\frac{3}{2})$	$2p_{1/2}2p_{3/2}5d_{3/2}(J=\frac{5}{2})$
N49	8.935(3)	7.3	N	8.947	2.5	$2s_{1/2}2p^2_{3/2}(J=\frac{5}{2})$	$2s_{1/2}2p_{3/2}6d_{3/2}(J=\frac{5}{2})$
N50,C27	8.843(3)	10.5	C	8.859	3.3	$2s_{1/2}2p_{3/2}(J=1)$	$2s_{1/2}5d_{5/2}(J=2)$
			N	8.845	2.7	$2p_{1/2}2p^2_{3/2}(J=\frac{3}{2})$	$6d_{5/2}(J=\frac{5}{2})$
N51	8.812(3)	7.9	N	8.819	4.1	$2p_{3/2}(J=\frac{3}{2})$	$2s_{1/2}2p_{3/2}5p_{3/2}(J=\frac{5}{2})$
			N	8.819	2.8	$2p_{3/2}(J=\frac{3}{2})$	$2s_{1/2}2p_{3/2}5p_{3/2}(J=\frac{3}{2})$
N52	8.779(3)	12.3	N	8.787	3.0	$2p_{1/2}2p^2_{3/2}(J=\frac{3}{2})$	$2p_{1/2}2p_{3/2}6d_{5/2}(J=\frac{5}{2})$
			N	8.781	2.0	$2p_{1/2}2p^2_{3/2}(J=\frac{5}{2})$	$2p_{1/2}2p_{3/2}6d_{5/2}(J=\frac{7}{2})$
			N	8.818	1.2	$2p_{3/2}(J=\frac{3}{2})$	$2s_{1/2}2p_{3/2}5p_{3/2}(J=\frac{1}{2})$
N53	8.732(3)	9.2	N	8.736	5.4	$2p_{3/2}(J=\frac{3}{2})$	$6d_{5/2}(J=\frac{5}{2})$
N54	8.676(3)	11.7	N	8.682	5.3	$2p_{3/2}(J=\frac{3}{2})$	$2p_{1/2}2p_{3/2}6d_{3/2}(J=\frac{5}{2})$
N55	8.642(2)	28.0	N	8.648	7.2	$2p_{3/2}(J=\frac{3}{2})$	$2p_{1/2}2p_{3/2}6d_{3/2}(J=\frac{3}{2})$
			N	8.648	4.8	$2p_{3/2}(J=\frac{3}{2})$	$2p_{1/2}2p_{3/2}6d_{3/2}(J=\frac{1}{2})$
N56	8.587(4)	5.2	N	8.595	1.6	$2p_{1/2}2p^2_{3/2}(J=\frac{3}{2})$	$7d_{5/2}(J=\frac{5}{2})$
N57	8.529(4)	5.1	N	8.540	1.8	$2p_{1/2}2p^2_{3/2}(J=\frac{3}{2})$	$2p_{1/2}2p_{3/2}7d_{5/2}(J=\frac{5}{2})$
			N	8.536	1.2	$2p_{1/2}2p^2_{3/2}(J=\frac{5}{2})$	$2p_{1/2}2p_{3/2}7d_{5/2}(J=\frac{7}{2})$
N58	8.435(3)	9.5	N	8.440	3.0	$2p_{3/2}(J=\frac{3}{2})$	$2p_{1/2}2p_{3/2}7d_{3/2}(J=\frac{5}{2})$
			N	8.441	1.0	$2p_{3/2}(J=\frac{3}{2})$	$2p_{1/2}2p_{3/2}7d_{3/2}(J=\frac{3}{2})$
N59	8.401(3)	17.7	N	8.409	3.8	$2p_{3/2}(J=\frac{3}{2})$	$2p_{1/2}2p_{3/2}7d_{3/2}(J=\frac{3}{2})$
			N	8.408	2.6	$2p_{3/2}(J=\frac{3}{2})$	$2p_{1/2}2p_{3/2}7d_{3/2}(J=\frac{1}{2})$
N60	8.389(5)	4.7	N	8.401	1.8	$2p_{3/2}(J=\frac{3}{2})$	$2s_{1/2}2p_{3/2}6p_{3/2}(J=\frac{5}{2})$
			N	8.401	1.3	$2p_{3/2}(J=\frac{3}{2})$	$2s_{1/2}2p_{3/2}6p_{3/2}(J=\frac{3}{2})$

Table 3—Continued

Label	$\lambda_{\rm exp}$[a]	Iexp [b]	Ion [c]	$\lambda_{\rm FAC}$ [d]	$I_{\rm FAC}$ [e]	Lower [f]	Upper [g]

[a]Measured wavelength in Å. Numbers in the parentheses are the estimated uncertainties in mÅ.

[b]Measured relative intensities, normalized to 100, the strongest line for each charge state.

[c]Ion charge state. For example, N indicate N-like ions

[d]Calculated wavelengths (in Å) using configuration interaction theory using FAC code.

[e]Calculated relative intensity.

[f]Configuration labels for the lower levels.

[g]Configuration labels for the upper levels.

[i]Wavelength from Fawcett, B. C., Jordan, C., Lemen, J. R., & Phillips, K. J. H. 1987, Mon. Not. R. astr. Soc., 225, 1013

[j]Wavelength from McKenzie, D. L., Landecker, P. B., Feldman, U.,& Doschek, G. A., 1985, ApJ, 289, 849

Table 4. C-like Fe XXI lines

Label	$\lambda_{\rm exp}$[a]	$I_{\rm exp}$ [b]	Ion [c]	$\lambda_{\rm FAC}$ [d]	$I_{\rm FAC}$ [e]	Lower [f]	Upper [g]
C14	9.981(6)	14.2	C	9.986	12.0	$2s_{1/2}2p_{3/2}(J=1)$	$2s_{1/2}4s_{1/2}(J=0)$
C15	9.807(6)	21.1	C	9.817	21.4	$2s_{1/2}2p_{3/2}(J=1)$	$2s_{1/2}4d_{5/2}(J=2)$
C16	9.758(9)	4.4	C	9.759	2.9	$2p_{1/2}2p_{3/2}(J=2)$	$2p_{1/2}4s_{1/2}(J=1)$
			C	9.766	0.3	$2p^2_{3/2}(J=2)$	$2p_{3/2}4s_{1/2}(J=1)$
C17	9.693(6)	13.1	C	9.700	4.0	$2p^2_{3/2}(J=0)$	$2p_{3/2}4d_{5/2}(J=1)$
			C	9.703	3.7	$2s_{1/2}2p_{1/2}2p^2_{3/2}(J=1)$	$2s_{1/2}2p_{1/2}2p_{3/2}4d_{5/2}(J=2)$
C18	9.583(6)	10.4	C	9.591	5.7	$2p_{1/2}2p_{3/2}(J=2)$	$2p_{1/2}4d_{5/2}(J=3)$
	9.587 [i]						
C19	9.548(6)	24.1	C	9.546	9.5	$2p_{1/2}2p_{3/2}(J=1)$	$2p_{1/2}4d_{3/2}(J=1)$
			C	9.552	7.9	$2p_{1/2}2p_{3/2}(J=1)$	$2p_{1/2}4d_{5/2}(J=2)$
	9.542 [i]						
	9.548 [i]						
C20	9.473(5)	100.0	C	9.480	91.8	$2p^2_{1/2}(J=0)$	$2p_{1/2}4d_{3/2}(J=1)$
	9.482 [i]						
C21	9.185(5)	29.9	C	9.194	21.7	$2p^2_{1/2}(J=0)$	$2s_{1/2}4p_{3/2}(J=1)$
C22	8.919(2)	3.1	C	8.929	3.7	$2s_{1/2}2p_{3/2}(J=1)$	$2s_{1/2}5s_{1/2}(J=0)$
C23	8.888(3)	1.2	C	8.887	0.7	$2p_{1/2}2p_{3/2}(J=1)$	$2s_{1/2}2p_{1/2}2p_{3/2}4p_{3/2}(J=2)$
			C	8.883	0.4	$2p_{1/2}2p_{3/2}(J=1)$	$2s_{1/2}2p_{1/2}2p_{3/2}4p_{3/2}(J=1)$
C24	8.856(3)	2.8	C	8.861	2.2	$2p^2_{3/2}(J=0)$	$2p_{1/2}5d_{3/2}(J=1)$
			C	8.870	0.6	$2s_{1/2}2p_{1/2}2p^2_{3/2}(J=2)$	$2s_{1/2}5d_{5/2}(J=3)$
C25	8.850(2)	6.8	C	8.859	7.9	$2s_{1/2}2p_{3/2}(J=1)$	$2s_{1/2}5d_{5/2}(J=2)$
C26	8.758(2)	3.6	C	8.764	2.3	$2p^2_{3/2}(J=0)$	$2p_{3/2}5d_{5/2}(J=1)$
			C	8.761	1.4	$2s_{1/2}2p_{1/2}2p^2_{3/2}(J=1)$	$2s_{1/2}2p_{1/2}2p_{3/2}5d_{5/2}(J=2)$
C27,N50	8.839(3)	1.7	C	8.840	0.6	$2p^2_{1/2}(J=0)$	$2s_{1/2}2p_{1/2}2p_{3/2}4p_{1/2}(J=1)$
			N	8.845	0.3	$2p_{1/2}2p^2_{3/2}(J=\frac{3}{2})$	$6d_{5/2}(J=\frac{5}{2})$
C28	8.827(3)	1.8	C	8.826	1.1	$2p^2_{1/2}(J=0)$	$2s_{1/2}2p_{1/2}2p_{3/2}4p_{3/2}(J=1)$
C29,N53	8.732(4)	1.0	C	8.734	0.9	$2p_{1/2}2p_{3/2}(J=2)$	$2p_{1/2}5s_{1/2}(J=1)$
			N	8.736	0.7	$2p_{3/2}(J=\frac{3}{2})$	$6d_{5/2}(J=\frac{5}{2})$
C30	8.695(20)	0.1	C	8.704	0.5	$2s_{1/2}2p_{3/2}(J=2)$	$2s_{1/2}5s_{1/2}(J=1)$
			C	8.702	0.3	$2p_{1/2}2p_{3/2}(J=1)$	$2p_{1/2}5s_{1/2}(J=0)$
			C	8.701	0.2	$2p_{1/2}2p_{3/2}(J=1)$	$2p_{1/2}5s_{1/2}(J=1)$
C31	8.660(2)	6.9	C	8.666	4.3	$2p_{1/2}2p_{3/2}(J=2)$	$2p_{1/2}5d_{5/2}(J=3)$
	8.663 [h]						
C32	8.639(2)	6.1	C	8.639	3.1	$2s_{1/2}2p_{3/2}(J=2)$	$2s_{1/2}5d_{5/2}(J=3)$
	8.640 [h]						
C33	8.627(2)	11.4	C	8.635	7.6	$2p_{1/2}2p_{3/2}(J=1)$	$2p_{1/2}5d_{5/2}(J=2)$
C34	8.569(2)	35.1	C	8.578	35.6	$2p^2_{1/2}(J=0)$	$2p_{1/2}5d_{3/2}(J=1)$
	8.5740(8) [h]						
	8.573 [i]						
C35	8.516(3)	1.6	C	8.522	0.7	$2s_{1/2}2p_{3/2}(J=1)$	$2s_{1/2}2p_{1/2}2p_{3/2}5d_{3/2}(J=2)$
			C	8.521	0.4	$2s_{1/2}2p_{1/2}2p^2_{3/2}(J=2)$	$2s_{1/2}2p_{1/2}2p_{3/2}5d_{5/2}(J=3)$
C36,N58	8.435(3)	3.1	C	8.450	1.5	$2s_{1/2}2p_{3/2}(J=1)$	$2s_{1/2}6s_{1/2}(J=0)$
			N	8.440	0.2	$2p_{3/2}(J=\frac{3}{2})$	$2p_{1/2}2p_{3/2}7d_{3/2}(J=\frac{5}{2})$
C37	8.403(2)	5.6	C	8.414	3.5	$2s_{1/2}2p_{3/2}(J=1)$	$2s_{1/2}6d_{5/2}(J=2)$
			C	8.413	1.2	$2p^2_{3/2}(J=0)$	$2p_{1/2}6d_{3/2}(J=1)$
C38	8.374(5)	0.9	C	8.373	0.5	$2p_{1/2}2p_{3/2}(J=1)$	$2s_{1/2}5p_{3/2}(J=2)$

Table 4—Continued

Label	$\lambda_{\rm exp}$[a]	Iexp [b]	Ion [c]	$\lambda_{\rm FAC}$ [d]	$I_{\rm FAC}$ [e]	Lower [f]	Upper [g]
C39	8.321(3)	2.7	C	8.328	1.2	$2p^2_{3/2}(J=0)$	$2p_{3/2}6d_{5/2}(J=1)$
C40	8.313(2)	9.2	C	8.317	8.7	$2p^2_{1/2}(J=0)$	$2s_{1/2}5p_{3/2}(J=1)$
C41	8.234(3)	4.8	C	8.237	2.2	$2p_{1/2}2p_{3/2}(J=2)$	$2p_{1/2}6d_{5/2}(J=3)$
C42	8.206(2)	8.8	C	8.208	4.0	$2p_{1/2}2p_{3/2}(J=1)$	$2p_{1/2}6d_{5/2}(J=2)$
	8.2036(9) [h]						
C43	8.180(4)	2.0	C	8.189	0.8	$2s_{1/2}2p_{3/2}(J=1)$	$2s_{1/2}7s_{1/2}(J=0)$
C44	8.156(2)	22.8	C	8.158	16.2	$2p^2_{1/2}(J=0)$	$2p_{1/2}6d_{3/2}(J=1)$
	8.1536(5) [h]						
C45 [bl1]	8.081(3)	4.5	C	8.085	0.6	$2p^2_{3/2}(J=0)$	$2p_{3/2}7d_{5/2}(J=1)$
C46	8.009(3)	3.8	C	8.013	0.5	$2p^2_{1/2}(J=0)$	$2s_{1/2}2p_{1/2}2p_{3/2}5p_{3/2}(J=1)$
			C	8.012	0.3	$2p^2_{3/2}(J=0)$	$2p_{1/2}8d_{3/2}(J=1)$
C47	7.997(3)	5.1	C	7.999	1.3	$2p_{1/2}2p_{3/2}(J=2)$	$2p_{1/2}7d_{5/2}(J=3)$
C48	7.969(3)	4.2	C	7.971	2.4	$2p_{1/2}2p_{3/2}(J=1)$	$2p_{1/2}7d_{5/2}(J=2)$
C49	7.920(2)	11.8	C	7.924	8.7	$2p^2_{1/2}(J=0)$	$2p_{1/2}7d_{3/2}(J=1)$
C50	7.906(3)	5.0	C	7.912	3.8	$2p^2_{1/2}(J=0)$	$2s_{1/2}6p_{3/2}(J=1)$
C51	7.847(3)	4.0	C	7.851	0.6	$2p_{1/2}2p_{3/2}(J=2)$	$2p_{1/2}8d_{5/2}(J=3)$
C52	7.820(4)	2.5	C	7.825	1.0	$2p_{1/2}2p_{3/2}(J=1)$	$2p_{1/2}8d_{5/2}(J=2)$
			C	7.824	0.5	$2p_{1/2}2p_{3/2}(J=1)$	$2p_{1/2}8d_{3/2}(J=1)$
			C	7.828	0.4	$2s_{1/2}2p_{3/2}(J=2)$	$2s_{1/2}8d_{5/2}(J=3)$
C53	7.773(3)	4.2	C	7.780	3.3	$2p^2_{1/2}(J=0)$	$2p_{1/2}8d_{3/2}(J=1)$
C54	7.756(3)	3.0	C	7.754	0.4	$2p_{1/2}2p_{3/2}(J=2)$	$2p_{1/2}9d_{5/2}(J=3)$
C55	7.678(3)	6.2	C	7.684	2.1	$2p^2_{1/2}(J=0)$	$2p_{1/2}9d_{3/2}(J=1)$
			C	7.687	2.0	$2p^2_{1/2}(J=0)$	$2s_{1/2}7p_{3/2}(J=1)$
C56	7.662(10)	0.7	C	7.660	0.5	$2p_{1/2}2p_{3/2}(J=1)$	$2p_{1/2}10d_{5/2}(J=2)$
C57	7.611(4)	2.2	C	7.617	1.5	$2p^2_{1/2}(J=0)$	$2p_{1/2}10d_{3/2}(J=1)$

[a]Measured wavelength in Å. Numbers in the parentheses are the estimated uncertainties in mÅ.

[b]Measured relative intensities, normalized to 100, the strongest line for each charge state.

[c]Ion charge state. For example, N indicate N-like ions

[d]Calculated wavelengths (in Å) using configuration interaction theory using FAC code.

[e]Calculated relative intensity.

[f]Configuration labels for the lower levels.

[g]Configuration labels for the upper levels.

[h]Wavelength from Wargelin, B. J., Beiersdorfer, P., Liedahl, D. A., Kahn, S. M., & von Goeler, S., 1998, ApJ496, 1031

[i]Wavelength from Fawcett, B. C., Jordan, C., Lemen, J. R., & Phillips, K. J. H. 1987, Mon. Not. R. astr. Soc., 225, 1013

[bl1]Blended with B47, see Table 5

Table 5. B-like Fe XXII lines

Label	$\lambda_{\rm exp}$[a]	$I_{\rm exp}$ [b]	Ion [c]	$\lambda_{\rm FAC}$ [d]	$I_{\rm FAC}$ [e]	Lower [f]	Upper [g]
B21	9.380(6)	27.3	B	9.392	15.6	$2s_{1/2}2p_{1/2}2p_{3/2}(J=\frac{3}{2})$	$2s_{1/2}2p_{1/2}4s_{1/2}(J=\frac{1}{2})$
B22	9.356(6)	11.1	B	9.371	11.5	$2s_{1/2}2p_{1/2}2p_{3/2}(J=\frac{1}{2})$	$2s_{1/2}2p_{1/2}4d_{5/2}(J=\frac{3}{2})$
B23	9.246(6)	16.0	B	9.261	19.3	$2s_{1/2}2p_{1/2}2p_{3/2}(J=\frac{3}{2})$	$2s_{1/2}2p_{1/2}4d_{5/2}(J=\frac{5}{2})$
B24	9.068(2)	30.5	B	9.074	23.5	$2p_{3/2}(J=\frac{3}{2})$	$4d_{5/2}(J=\frac{5}{2})$
			B	9.077	12.3	$2p_{3/2}(J=\frac{3}{2})$	$4d_{3/2}(J=\frac{3}{2})$
B25	9.061(2)	12.4	B	9.063	7.7	$2s_{1/2}2p_{1/2}2p_{3/2}(J=\frac{3}{2})$	$2s_{1/2}2p_{1/2}4d_{5/2}(J=\frac{5}{2})$
B26	9.043(3)	4.3	B	9.046	4.8	$2s_{1/2}2p_{1/2}2p_{3/2}(J=\frac{3}{2})$	$2s_{1/2}2p_{1/2}4d_{3/2}(J=\frac{5}{2})$
B27	9.023(2)	5.9	B	9.022	5.1	$2s_{1/2}2p_{1/2}2p_{3/2}(J=\frac{3}{2})$	$2s_{1/2}2p_{1/2}4d_{5/2}(J=\frac{5}{2})$
			B	9.028	2.3	$2s_{1/2}(J=\frac{1}{2})$	$2s_{1/2}2p_{1/2}4d_{3/2}(J=\frac{3}{2})$
B28	8.993(2)	8.0	B	8.995	4.0	$2s_{1/2}(J=\frac{1}{2})$	$2s_{1/2}2p_{1/2}4d_{3/2}(J=\frac{3}{2})$
			B	8.993	2.3	$2s_{1/2}(J=\frac{1}{2})$	$2s_{1/2}2p_{1/2}4d_{3/2}(J=\frac{1}{2})$
B29	8.977(2)	100.0	B	8.981	91.0	$2p_{1/2}(J=\frac{1}{2})$	$4d_{3/2}(J=\frac{3}{2})$
	8.9748(6) [h]						
	8.976[i]						
	8.975[j]						
B30	8.963(3)	6.5	B	8.961	3.4	$2s_{1/2}2p_{1/2}2p_{3/2}(J=\frac{3}{2})$	$2s_{1/2}2p_{3/2}4d_{3/2}(J=\frac{5}{2})$
B31,C28	8.828(3)	3.3	C	8.826	1.5	$2p^2_{1/2}(J=0)$	$2s_{1/2}2p_{1/2}2p_{3/2}4p_{3/2}(J=1)$
			B	8.833	1.3	$2p_{3/2}(J=\frac{3}{2})$	$2s_{1/2}2p_{1/2}4p_{1/2}(J=\frac{3}{2})$
B32,C26	8.759(2)	7.3	C	8.764	2.6	$2p^2_{3/2}(J=0)$	$2p_{3/2}5d_{5/2}(J=1)$
			B	8.766	2.4	$2p_{1/2}(J=\frac{1}{2})$	$2s_{1/2}2p_{1/2}4p_{1/2}(J=\frac{1}{2})$
			C	8.761	1.5	$2s_{1/2}2p_{1/2}2p^2_{3/2}(J=1)$	$2s_{1/2}2p_{1/2}2p_{3/2}5d_{5/2}(J=2)$
	8.753 [h]						
B33	8.738(2)	12.7	B	8.742	10.1	$2p_{1/2}(J=\frac{1}{2})$	$2s_{1/2}2p_{1/2}4p_{1/2}(J=\frac{3}{2})$
	8.736 [h]						
	8.734[i]						
B34	8.722(2)	10.3	B	8.726	10.9	$2p_{1/2}(J=\frac{1}{2})$	$2s_{1/2}2p_{1/2}4p_{3/2}(J=\frac{1}{2})$
	8.720 [h]						
	8.722[i]						
B35	8.714(2)	28.9	B	8.719	23.7	$2p_{1/2}(J=\frac{1}{2})$	$2s_{1/2}2p_{1/2}4p_{3/2}(J=\frac{3}{2})$
	8.714 [h]						
	8.715[i]						
B36,C37	8.403(2)	8.6	B	8.419	4.5	$2s_{1/2}2p_{1/2}2p_{3/2}(J=\frac{1}{2})$	$2s_{1/2}2p_{1/2}5d_{5/2}(J=\frac{3}{2})$
			C	8.414	4.0	$2s_{1/2}2p_{3/2}(J=1)$	$2s_{1/2}6d_{5/2}(J=2)$
	8.4053(6) [h]						
B37	8.370(3)	4.9	B	8.385	4.0	$2s_{1/2}2p_{1/2}2p_{3/2}(J=\frac{3}{2})$	$2s_{1/2}2p_{1/2}5s_{1/2}(J=\frac{1}{2})$
B38	8.344(3)	3.0	B	8.354	0.6	$2s_{1/2}2p^2_{3/2}(J=\frac{5}{2})$	$2s_{1/2}2p_{1/2}5d_{5/2}(J=\frac{7}{2})$
B39	8.326(3)	8.8	B	8.333	6.4	$2s_{1/2}2p_{1/2}2p_{3/2}(J=\frac{3}{2})$	$2s_{1/2}2p_{1/2}5d_{5/2}(J=\frac{5}{2})$
B40	8.375(3)	4.2	B	8.385	3.9	$2s_{1/2}2p_{1/2}2p_{3/2}(J=\frac{3}{2})$	$2s_{1/2}2p_{1/2}5s_{1/2}(J=\frac{1}{2})$
B41	8.181(3)	6.2	B	8.181	3.7	$2s_{1/2}2p_{1/2}2p_{3/2}(J=\frac{5}{2})$	$2s_{1/2}2p_{1/2}5d_{5/2}(J=\frac{7}{2})$
			B	8.184	1.0	$2s_{1/2}2p_{1/2}2p_{3/2}(J=\frac{5}{2})$	$2s_{1/2}2p_{1/2}5d_{3/2}(J=\frac{5}{2})$
B42	8.170(2)	23.2	B	8.173	13.6	$2p_{3/2}(J=\frac{3}{2})$	$5d_{5/2}(J=\frac{5}{2})$
			B	8.164	4.4	$2s_{1/2}2p_{1/2}2p_{3/2}(J=\frac{3}{2})$	$2s_{1/2}2p_{1/2}5d_{5/2}(J=\frac{5}{2})$
	8.1684(4) [h]						
B43	8.140(3)	3.2	B	8.139	2.0	$2s_{1/2}2p_{1/2}2p_{3/2}(J=\frac{3}{2})$	$2s_{1/2}2p_{1/2}5d_{5/2}(J=\frac{5}{2})$
B44	8.129(5)	1.6	B	8.132	1.3	$2s_{1/2}(J=\frac{1}{2})$	$2s_{1/2}2p_{1/2}5d_{3/2}(J=\frac{3}{2})$
			B	8.129	0.5	$2s_{1/2}2p_{1/2}2p_{3/2}(J=\frac{3}{2})$	$2s_{1/2}2p_{3/2}5s_{1/2}(J=\frac{1}{2})$

Table 5—Continued

Label	$\lambda_{\rm exp}$[a]	$I_{\rm exp}$ [b]	Ion [c]	$\lambda_{\rm FAC}$ [d]	$I_{\rm FAC}$ [e]	Lower [f]	Upper [g]
B45	8.109(3)	4.9	B	8.109	1.5	$2s_{1/2}(J=\frac{1}{2})$	$2s_{1/2}2p_{1/2}5d_{3/2}(J=\frac{3}{2})$
			B	8.108	1.0	$2s_{1/2}(J=\frac{1}{2})$	$2s_{1/2}2p_{1/2}5d_{3/2}(J=\frac{1}{2})$
B46	8.093(2)	29.0	B	8.097	32.0	$2p_{1/2}(J=\frac{1}{2})$	$5d_{3/2}(J=\frac{3}{2})$
	8.0904(3) [h]						
	8.091[i]						
B47,C45	8.081(3)	4.5	B	8.081	1.0	$2s_{1/2}2p_{1/2}2p_{3/2}(J=\frac{3}{2})$	$2s_{1/2}2p_{3/2}5d_{3/2}(J=\frac{5}{2})$
			C	8.085	0.6	$2p^2_{3/2}(J=0)$	$2p_{3/2}7d_{5/2}(J=1)$
B48,C47	7.997(4)	2.6	C	7.999	1.0	$2p_{1/2}2p_{3/2}(J=2)$	$2p_{1/2}7d_{5/2}(J=3)$
			B	8.006	0.6	$2s_{1/2}2p_{1/2}2p_{3/2}(J=\frac{1}{2})$	$2s_{1/2}2p_{1/2}6s_{1/2}(J=\frac{1}{2})$
			C	8.013	0.5	$2p^2_{1/2}(J=0)$	$2s_{1/2}2p_{1/2}2p_{3/2}5p_{3/2}(J=1)$
			C	8.012	0.2	$2p^2_{3/2}(J=0)$	$2p_{1/2}8d_{3/2}(J=1)$
B49,C48	7.969(3)	6.5	B	7.979	1.9	$2s_{1/2}2p_{1/2}2p_{3/2}(J=\frac{1}{2})$	$2s_{1/2}2p_{1/2}6d_{5/2}(J=\frac{3}{2})$
			C	7.971	1.8	$2p_{1/2}2p_{3/2}(J=1)$	$2p_{1/2}7d_{5/2}(J=2)$
B50,C50	7.903(4)	3.1	C	7.912	3.5	$2p^2_{1/2}(J=0)$	$2s_{1/2}6p_{3/2}(J=1)$
			B	7.902	2.7	$2s_{1/2}2p_{1/2}2p_{3/2}(J=\frac{3}{2})$	$2s_{1/2}2p_{1/2}6d_{5/2}(J=\frac{5}{2})$
			B	7.897	1.0	$2p_{1/2}(J=\frac{1}{2})$	$2s_{1/2}2p_{1/2}5p_{1/2}(J=\frac{1}{2})$
B51	7.865(2)	8.6	B	7.869	6.7	$2p_{1/2}(J=\frac{1}{2})$	$2s_{1/2}2p_{1/2}5p_{3/2}(J=\frac{3}{2})$
			B	7.871	3.5	$2p_{1/2}(J=\frac{1}{2})$	$2s_{1/2}2p_{1/2}5p_{3/2}(J=\frac{1}{2})$
	7.865 [h]						
B52	7.749(2)	13.1	B	7.756	7.3	$2p_{3/2}(J=\frac{3}{2})$	$6d_{5/2}(J=\frac{5}{2})$
	7.752 [h]						
B53	7.678(2)	19.5	B	7.687	14.7	$2p_{1/2}(J=\frac{1}{2})$	$6d_{3/2}(J=\frac{3}{2})$
	7.6812(4) [h]						
	7.682[j]						
B54	7.521(3)	12.5	B	7.525	3.6	$2p_{3/2}(J=\frac{3}{2})$	$7d_{5/2}(J=\frac{5}{2})$
B55	7.473(2)	3.3	B	7.476	2.7	$2p_{1/2}(J=\frac{1}{2})$	$2s_{1/2}2p_{1/2}6p_{3/2}(J=\frac{3}{2})$
			B	7.477	1.4	$2p_{1/2}(J=\frac{1}{2})$	$2s_{1/2}2p_{1/2}6p_{3/2}(J=\frac{1}{2})$
B56	7.455(2)	7.0	B	7.460	8.0	$2p_{1/2}(J=\frac{1}{2})$	$7d_{3/2}(J=\frac{3}{2})$
B57,C58	7.388(3)	2.0	C	7.392	0.6	$2p^2_{1/2}(J=0)$	$2s_{1/2}10p_{3/2}(J=1)$
			B	7.389	0.5	$2s_{1/2}2p_{1/2}2p_{3/2}(J=\frac{5}{2})$	$2s_{1/2}2p_{1/2}8d_{5/2}(J=\frac{7}{2})$
B58	7.380(2)	3.7	B	7.383	1.9	$2p_{3/2}(J=\frac{3}{2})$	$8d_{5/2}(J=\frac{5}{2})$
			B	7.383	0.7	$2p_{3/2}(J=\frac{3}{2})$	$8d_{3/2}(J=\frac{3}{2})$
B59?	7.356(3)	2.0	B	7.359	0.3	$2s_{1/2}2p_{1/2}2p_{3/2}(J=\frac{3}{2})$	$2s_{1/2}2p_{1/2}8d_{5/2}(J=\frac{5}{2})$
			B	7.352	0.2	$2s_{1/2}2p_{1/2}2p_{3/2}(J=\frac{3}{2})$	$2s_{1/2}2p_{1/2}10d_{5/2}(J=\frac{5}{2})$
B60	7.330(3)	1.4	B	7.330	0.2	$2s_{1/2}(J=\frac{1}{2})$	$2s_{1/2}2p_{1/2}8d_{3/2}(J=\frac{3}{2})$
			B	7.332	0.2	$2p_{3/2}(J=\frac{3}{2})$	$2s_{1/2}2p_{3/2}6p_{3/2}(J=\frac{5}{2})$
			B	7.330	0.2	$2s_{1/2}(J=\frac{1}{2})$	$2s_{1/2}2p_{1/2}8d_{3/2}(J=\frac{1}{2})$
B61	7.317(2)	4.9	B	7.319	3.8	$2p_{1/2}(J=\frac{1}{2})$	$8d_{3/2}(J=\frac{3}{2})$
B62	7.284(2)	2.9	B	7.288	1.3	$2p_{3/2}(J=\frac{3}{2})$	$2s^2_{1/2}9d_{5/2}(J=\frac{5}{2})$
			B	7.288	0.5	$2p_{3/2}(J=\frac{3}{2})$	$2s^2_{1/2}9d_{3/2}(J=\frac{3}{2})$
B63?	7.271(2)	8.1	B	7.275	0.7	$2p_{1/2}(J=\frac{1}{2})$	$2s_{1/2}2p_{1/2}7p_{3/2}(J=\frac{3}{2})$
B64	7.255(2)	2.6	B	7.258	1.4	$2p_{1/2}(J=\frac{1}{2})$	$2s_{1/2}2p_{1/2}7p_{3/2}(J=\frac{3}{2})$
			B	7.259	0.7	$2p_{1/2}(J=\frac{1}{2})$	$2s_{1/2}2p_{1/2}7p_{3/2}(J=\frac{1}{2})$
			B	7.261	0.3	$2p_{1/2}(J=\frac{1}{2})$	$2s_{1/2}2p_{1/2}7p_{1/2}(J=\frac{3}{2})$
B65	7.222(2)	4.4	B	7.227	2.5	$2p_{1/2}(J=\frac{1}{2})$	$2s^2_{1/2}9d_{3/2}(J=\frac{3}{2})$
			B	7.222	0.9	$2p_{3/2}(J=\frac{3}{2})$	$2s^2_{1/2}10d_{5/2}(J=\frac{5}{2})$

Table 5—Continued

Label	$\lambda_{\rm exp}$[a]	Iexp [b]	Ion [c]	$\lambda_{\rm FAC}$ [d]	$I_{\rm FAC}$ [e]	Lower [f]	Upper [g]
B66?	7.170(2)	3.1	B	7.173	0.1	$2s_{1/2}(J=\frac{1}{2})$	$2s_{1/2}2p_{1/2}10d_{3/2}(J=\frac{3}{2})$
			B	7.173	0.1	$2s_{1/2}(J=\frac{1}{2})$	$2s_{1/2}2p_{1/2}10d_{3/2}(J=\frac{1}{2})$
B67	7.159(3)	1.8	B	7.162	1.6	$2p_{1/2}(J=\frac{1}{2})$	$2s^2_{1/2}10d_{3/2}(J=\frac{3}{2})$
B68	7.137(3)	1.6	B	7.140	0.3	$2p_{1/2}(J=\frac{1}{2})$	$2s_{1/2}2p_{1/2}8p_{3/2}(J=\frac{3}{2})$
			B	7.141	0.2	$2p_{1/2}(J=\frac{1}{2})$	$2s_{1/2}2p_{1/2}8p_{1/2}(J=\frac{1}{2})$
B69	7.124(4)	0.8	B	7.124	0.6	$2p_{1/2}(J=\frac{1}{2})$	$2s_{1/2}2p_{1/2}8p_{3/2}(J=\frac{3}{2})$
			B	7.124	0.4	$2p_{1/2}(J=\frac{1}{2})$	$2s_{1/2}2p_{1/2}8p_{3/2}(J=\frac{1}{2})$
B70	7.047(3)	1.2	B	7.051	0.2	$2p_{1/2}(J=\frac{1}{2})$	$2s_{1/2}2p_{1/2}9p_{3/2}(J=\frac{3}{2})$
			B	7.052	0.1	$2p_{1/2}(J=\frac{1}{2})$	$2s_{1/2}2p_{1/2}9p_{1/2}(J=\frac{1}{2})$
B71	7.032(3)	1.8	B	7.036	0.3	$2p_{1/2}(J=\frac{1}{2})$	$2s_{1/2}2p_{1/2}9p_{3/2}(J=\frac{3}{2})$
			B	7.036	0.2	$2p_{1/2}(J=\frac{1}{2})$	$2s_{1/2}2p_{1/2}9p_{3/2}(J=\frac{1}{2})$
			B	7.037	0.1	$2p_{1/2}(J=\frac{1}{2})$	$2s_{1/2}2p_{1/2}9p_{1/2}(J=\frac{3}{2})$

[a]Measured wavelength in Å. Numbers in the parentheses are the estimated uncertainties in mÅ.

[b]Measured relative intensities, normalized to 100, the strongest line for each charge state.

[c]Ion charge state. For example, N indicate N-like ions

[d]Calculated wavelengths (in Å) using configuration interaction theory using FAC code.

[e]Calculated relative intensity.

[f]Configuration labels for the lower levels.

[g]Configuration labels for the upper levels.

[h]Wavelength from Wargelin, B. J., Beiersdorfer, P., Liedahl, D. A., Kahn, S. M., & von Goeler, S., 1998, ApJ496, 1031

[i]Wavelength from Fawcett, B. C., Jordan, C., Lemen, J. R., & Phillips, K. J. H. 1987, Mon. Not. R. astr. Soc., 225, 1013

[j]Wavelength from McKenzie, D. L., Landecker, P. B., Feldman, U.,& Doschek, G. A., 1985, ApJ, 289, 849

Table 6. Be-like Fe XXIII lines

Label	$\lambda_{\rm exp}$[a]	Iexp [b]	Ion [c]	$\lambda_{\rm FAC}$ [d]	$I_{\rm FAC}$ [e]	Lower [f]	Upper [g]
Be8	11.016(5)	89.2	Be	11.021	71.8	$2s^2_{1/2}(J=0)$	$2s_{1/2}3p_{1/2}(J=1)$
Be9	10.978(5)	100.0	Be	10.983	114.3	$2s^2_{1/2}(J=0)$	$2s_{1/2}3p_{3/2}(J=1)$
Be10	8.908(6)	8.1	Be	8.915	7.6	$2s_{1/2}2p_{3/2}(J=1)$	$2s_{1/2}4s_{1/2}(J=0)$
	8.906[h]						
	8.906[i]						
Be11	8.819(5)	23.9	Be	8.823	20.6	$2s_{1/2}2p_{3/2}(J=1)$	$2s_{1/2}4d_{5/2}(J=2)$
Be12	8.920(2)	2.4	Be	8.928	1.4	$2p^2_{3/2}(J=0)$	$2p_{3/2}4d_{5/2}(J=1)$
Be13	8.907(2)	9.9	Be	8.915	9.4	$2s_{1/2}2p_{3/2}(J=1)$	$2s_{1/2}4s_{1/2}(J=0)$
Be14	8.816(2)	25.7	Be	8.823	25.2	$2s_{1/2}2p_{3/2}(J=1)$	$2s_{1/2}4d_{5/2}(J=2)$
	8.8149(4)[h]						
	8.815[i]						
	8.811[j]						
Be15	8.705(3)	1.0	Be	8.709	1.5	$2s_{1/2}2p_{3/2}(J=2)$	$2s_{1/2}4s_{1/2}(J=1)$
Be16,C31	8.667(2)	2.7	C	8.666	1.0	$2p_{1/2}2p_{3/2}(J=2)$	$2p_{1/2}5d_{5/2}(J=3)$
			Be	8.672	0.9	$2p^2_{1/2}(J=0)$	$2p_{1/2}4d_{3/2}(J=1)$
Be17,C32	8.634(3)	1.2	Be	8.640	0.8	$2s_{1/2}2p_{1/2}(J=1)$	$2s_{1/2}4s_{1/2}(J=1)$
			C	8.639	0.7	$2s_{1/2}2p_{3/2}(J=2)$	$2s_{1/2}5d_{5/2}(J=3)$
Be18	8.613(2)	11.0	Be	8.618	8.4	$2s_{1/2}2p_{3/2}(J=2)$	$2s_{1/2}4d_{5/2}(J=3)$
	8.6172(6)[h]						
	8.616[i]						
	8.619[j]						
Be19	8.545(2)	5.5	Be	8.552	4.6	$2s_{1/2}2p_{1/2}(J=1)$	$2s_{1/2}4d_{3/2}(J=2)$
	8.546[h]						
	8.550[i]						
Be20	8.523(2)	2.3	Be	8.531	2.5	$2s_{1/2}2p_{1/2}(J=0)$	$2s_{1/2}4d_{3/2}(J=1)$
	8.529[h]						
Be21,C39	8.317(2)	5.3	Be	8.318	5.1	$2s^2_{1/2}(J=0)$	$2s_{1/2}4p_{1/2}(J=1)$
			C	8.317	3.1	$2p^2_{1/2}(J=0)$	$2s_{1/2}5p_{3/2}(J=1)$
Be22	8.305(2)	17.5	Be	8.306	28.5	$2s^2_{1/2}(J=0)$	$2s_{1/2}4p_{3/2}(J=1)$
	8.3038(3)[h]						
	8.305[i]						
	8.305[j]						
Be23	7.939(3)	3.2	Be	7.946	2.8	$2s_{1/2}2p_{3/2}(J=1)$	$2s_{1/2}5s_{1/2}(J=0)$
	7.936[h]						
Be24	7.901(2)	9.6	Be	7.909	7.4	$2s_{1/2}2p_{3/2}(J=1)$	$2s_{1/2}5d_{5/2}(J=2)$
	7.9009(5)[h]						
	7.902[i]						
Be25	7.733(2)	4.7	Be	7.737	3.6	$2s_{1/2}2p_{3/2}(J=2)$	$2s_{1/2}5d_{5/2}(J=3)$
	7.733[h]						
Be27	7.504(3)	2.9	Be	7.506	1.2	$2s_{1/2}2p_{3/2}(J=1)$	$2s_{1/2}6s_{1/2}(J=0)$
	7.498[h]						
Be28	7.474(2)	10.7	Be	7.474	9.5	$2s^2_{1/2}(J=0)$	$2s_{1/2}5p_{3/2}(J=1)$
	7.478[h]						
Be29	7.332(2)	4.0	Be	7.331	1.9	$2s_{1/2}2p_{3/2}(J=2)$	$2s_{1/2}6d_{5/2}(J=3)$
Be30,B67	7.282(2)	3.8	Be	7.282	1.0	$2s_{1/2}2p_{1/2}(J=1)$	$2s_{1/2}6d_{3/2}(J=2)$
			B	7.288	0.7	$2p_{3/2}(J=\frac{3}{2})$	$2s^2_{1/2}9d_{5/2}(J=\frac{5}{2})$

Table 6—Continued

Label	$\lambda_{\rm exp}$[a]	$I_{\rm exp}$ [b]	Ion [c]	$\lambda_{\rm FAC}$ [d]	$I_{\rm FAC}$ [e]	Lower [f]	Upper [g]
Be31	7.259(2)	1.7	Be	7.265	0.6	$2s_{1/2}2p_{3/2}(J=1)$	$2s_{1/2}7s_{1/2}(J=0)$
			Be	7.266	0.5	$2s_{1/2}2p_{1/2}(J=0)$	$2s_{1/2}6d_{3/2}(J=1)$
Be32,B69	7.249(2)	2.2	Be	7.254	1.6	$2s_{1/2}2p_{3/2}(J=1)$	$2s_{1/2}7d_{5/2}(J=2)$
			B	7.258	0.9	$2p_{1/2}(J=\frac{1}{2})$	$2s_{1/2}2p_{1/2}7p_{3/2}(J=\frac{3}{2})$
Be33?	7.113(3)	1.6	Be	7.110	0.7	$2s_{1/2}2p_{3/2}(J=1)$	$2s_{1/2}8d_{5/2}(J=2)$
			Be	7.118	0.4	$2s_{1/2}2p_{3/2}(J=1)$	$2s_{1/2}8s_{1/2}(J=0)$
Be34?	7.106(2)	3.6	Be	7.107	1.1	$2s_{1/2}2p_{3/2}(J=2)$	$2s_{1/2}7d_{5/2}(J=3)$
			Be	7.094	0.5	$2s^2_{1/2}(J=0)$	$2s_{1/2}6p_{1/2}(J=1)$
Be35	7.091(2)	7.5	Be	7.091	4.3	$2s^2_{1/2}(J=0)$	$2s_{1/2}6p_{3/2}(J=1)$
Be36?	7.012(3)	1.3	Be	7.015	0.4	$2s_{1/2}2p_{3/2}(J=1)$	$2s_{1/2}9d_{5/2}(J=2)$

[a]Measured wavelength in Å. Numbers in the parentheses are the estimated uncertainties in mÅ.

[b]Measured relative intensities, normalized to 100, the strongest line for each charge state.

[c]Ion charge state. For example, N indicate N-like ions

[d]Calculated wavelengths (in Å) using configuration interaction theory using FAC code.

[e]Calculated relative intensity.

[f]Configuration labels for the lower levels.

[g]Configuration labels for the upper levels.

[h]Wavelength from Wargelin, B. J., Beiersdorfer, P., Liedahl, D. A., Kahn, S. M., & von Goeler, S., 1998, ApJ496, 1031

[i]Wavelength from Fawcett, B. C., Jordan, C., Lemen, J. R., & Phillips, K. J. H. 1987, Mon. Not. R. astr. Soc., 225, 1013

[j]Wavelength from McKenzie, D. L., Landecker, P. B., Feldman, U.,& Doschek, G. A., 1985, ApJ, 289, 849

Table 7. Li-like Fe XXIV lines

Label	$\lambda_{\rm exp}$[a]	Iexp [b]	Ion [c]	$\lambda_{\rm FAC}$ [d]	$I_{\rm FAC}$ [e]	Lower [f]	Upper [g]
Li5	10.669(5)	46.1	Li	10.663	26.7	$2s_{1/2}(J=\frac{1}{2})$	$3p_{1/2}(J=\frac{1}{2})$
Li6	10.630(5)	100.0	Li	10.620	61.5	$2s_{1/2}(J=\frac{1}{2})$	$3p_{3/2}(J=\frac{3}{2})$
Li7	8.373(2)	4.3	Li	8.378	3.2	$2p_{3/2}(J=\frac{3}{2})$	$4s_{1/2}(J=\frac{1}{2})$
	8.3761(7)[h]						
	8.376[i]						
Li8,Be21	8.319(2)	21.6	Li	8.320	13.2	$2p_{3/2}(J=\frac{3}{2})$	$4d_{5/2}(J=\frac{5}{2})$
			Be	8.318	7.6	$2s^2_{1/2}(J=0)$	$2s_{1/2}4p_{1/2}(J=1)$
	8.3161(3)[h]						
	8.317[i]						
	8.318[j]						
Li9	8.288(3)	3.4	Li	8.289	1.9	$2p_{1/2}(J=\frac{1}{2})$	$4s_{1/2}(J=\frac{1}{2})$
	8.2850(4)[h]						
Li10	8.233(2)	8.5	Li	8.235	7.7	$2p_{1/2}(J=\frac{1}{2})$	$4d_{3/2}(J=\frac{3}{2})$
	8.2326(4)[h]						
	8.232[i]						
	8.233[j]						
Li11	7.998(3)	6.1	Li	7.998	4.5	$2s_{1/2}(J=\frac{1}{2})$	$4p_{1/2}(J=\frac{1}{2})$
	7.9960(4)[h]						
	7.996[i]						
	7.996[j]						
Li12	7.988(2)	16.3	Li	7.988	12.2	$2s_{1/2}(J=\frac{1}{2})$	$4p_{3/2}(J=\frac{3}{2})$
	7.9857(2)[h]						
	7.986[i]						
	7.986[j]						
Li13	7.461(2)	1.8	Li	7.463	1.2	$2p_{3/2}(J=\frac{3}{2})$	$5s_{1/2}(J=\frac{1}{2})$
	7.457[h]						
Li14	7.437(2)	4.1	Li	7.439	4.3	$2p_{3/2}(J=\frac{3}{2})$	$5d_{5/2}(J=\frac{5}{2})$
	7.437[h]						
Li15	7.389(3)	1.3	Li	7.392	0.6	$2p_{1/2}(J=\frac{1}{2})$	$5s_{1/2}(J=\frac{1}{2})$
Li16	7.369(2)	2.2	Li	7.370	2.5	$2p_{1/2}(J=\frac{1}{2})$	$5d_{3/2}(J=\frac{3}{2})$
Li17	7.168(2)	5.2	Li	7.166	4.0	$2s_{1/2}(J=\frac{1}{2})$	$5p_{3/2}(J=\frac{3}{2})$
			Li	7.170	1.4	$2s_{1/2}(J=\frac{1}{2})$	$5p_{1/2}(J=\frac{1}{2})$
Li18	7.046(3)	1.2	Li	7.046	0.5	$2p_{3/2}(J=\frac{3}{2})$	$6s_{1/2}(J=\frac{1}{2})$
Li19	7.034(2)	2.2	Li	7.034	1.9	$2p_{3/2}(J=\frac{3}{2})$	$6d_{5/2}(J=\frac{5}{2})$
Li20	6.973(2)	2.1	Li	6.972	1.1	$2p_{1/2}(J=\frac{1}{2})$	$6d_{3/2}(J=\frac{3}{2})$

[a]Measured wavelength in Å. Numbers in the parentheses are the estimated uncertainties in mÅ.

[b]Measured relative intensities, normalized to 100, the strongest line for each charge state.

[c]Ion charge state. For example, N indicate N-like ions

[d]Calculated wavelengths (in Å) using configuration interaction theory using FAC code.

[e]Calculated relative intensity.

[f]Configuration labels for the lower levels.

[g]Configuration labels for the upper levels.

[h]Wavelength from Wargelin, B. J., Beiersdorfer, P., Liedahl, D. A., Kahn, S. M., & von Goeler, S., 1998, ApJ496, 1031

[i]Wavelength from Fawcett, B. C., Jordan, C., Lemen, J. R., & Phillips, K. J. H. 1987, Mon. Not. R. astr. Soc., 225, 1013

[j]Wavelength from McKenzie, D. L., Landecker, P. B., Feldman, U.,& Doschek, G. A., 1985, ApJ, 289, 849

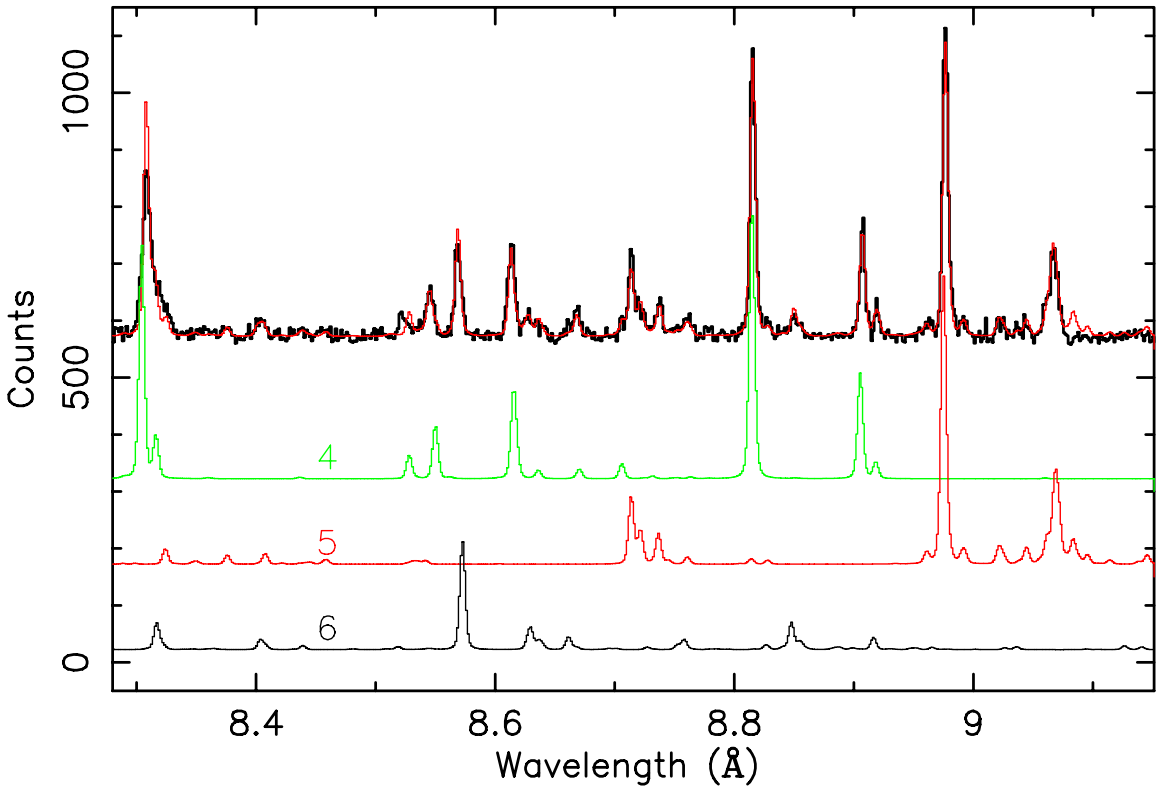

Fig. 1.— Fe spectral measurement at an electron beam energy of 1.95 keV and the FAC modeling in the 8–9 Åregion. The top black line is the measured data. The top red line is the best-fit theoretical model. The only free parameters in the model are the relative abundances of the three charge states. The bottom three curves show individual contributions from different charge states, with the labels indicating the number of electrons of the ions.

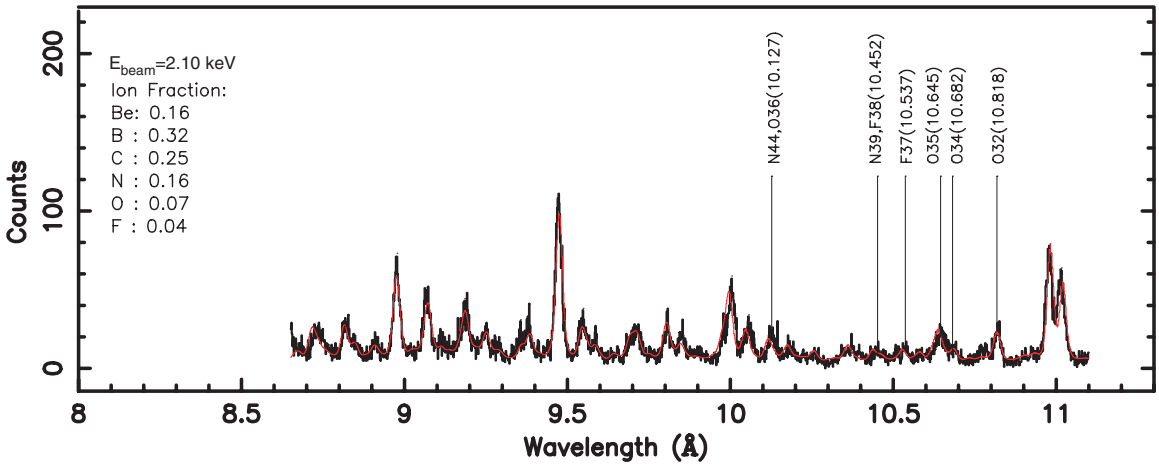

Fig. 2.— F-like Fe XVIII and O-like Fe XIX lines. The black line is the measured data. The red line is the best-fit theoretical model. The electron beam energy of the measurement and the ion charge balance from the model are listed.

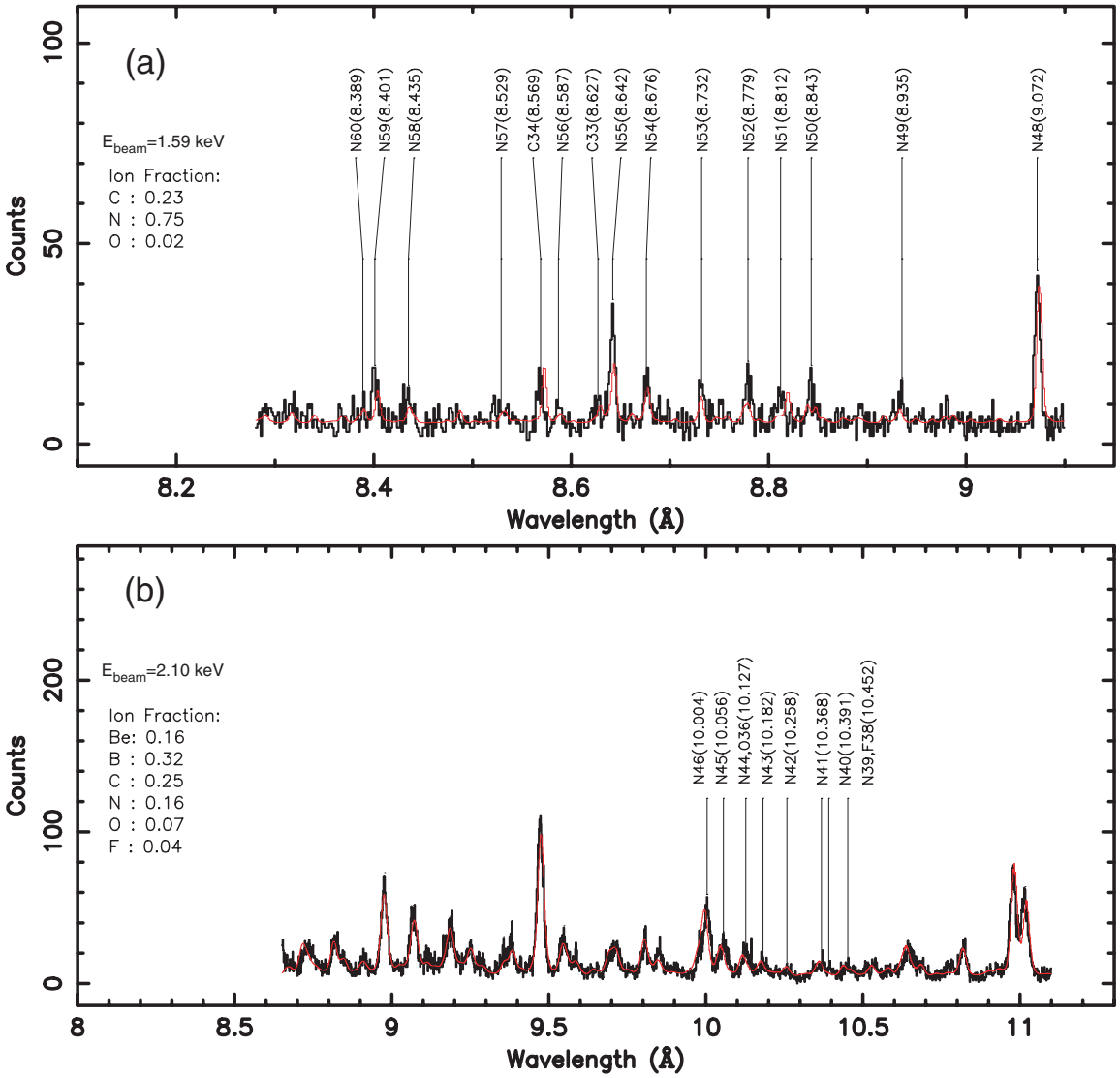

Fig. 3.— N-like Fe XX lines. The black line is the measured data. The red line is the best-fit theoretical model. The electron beam energy of the measurement and the ion charge balance from the model are listed.

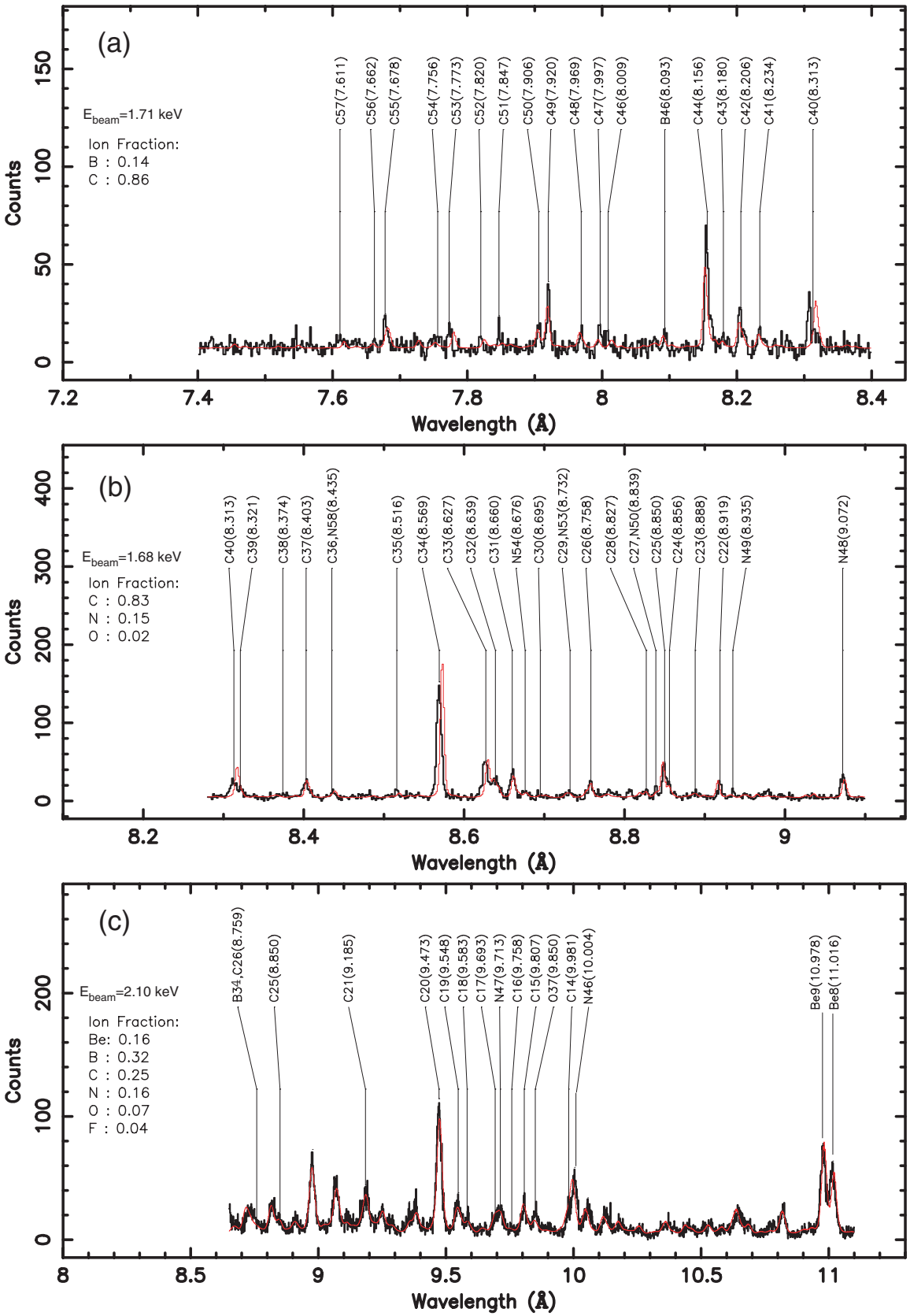

Fig. 4.— C-like Fe XXI lines. The black line is the measured data. The red line is the best-fit theoretical model. The electron beam energy of the measurement and the ion charge balance from the model are listed.

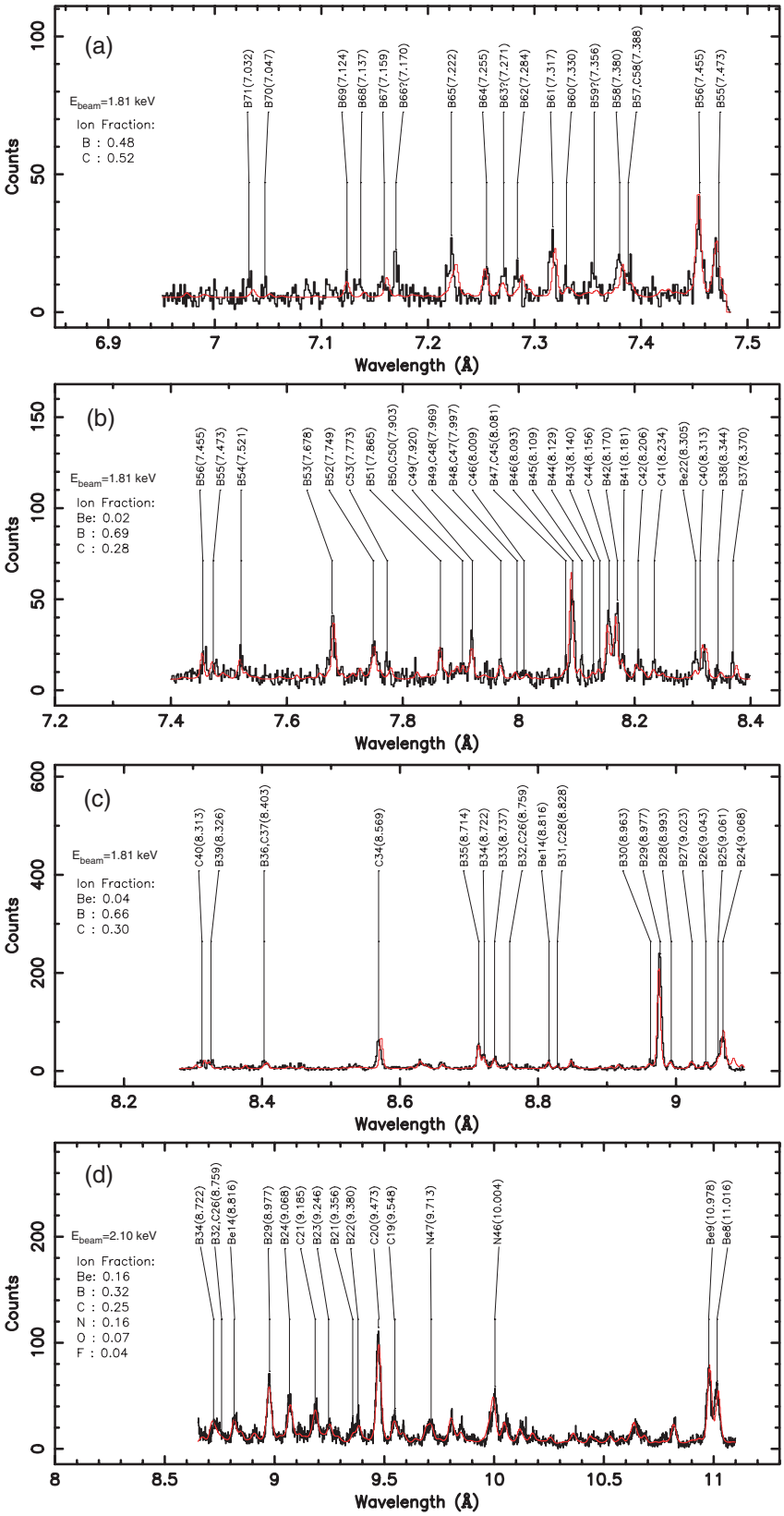

Fig. 5.— B-like Fe XXII lines. The black line is the measured data. The red line is the best-fit theoretical model. The electron beam energy of the measurement and the ion charge balance from the model are listed.

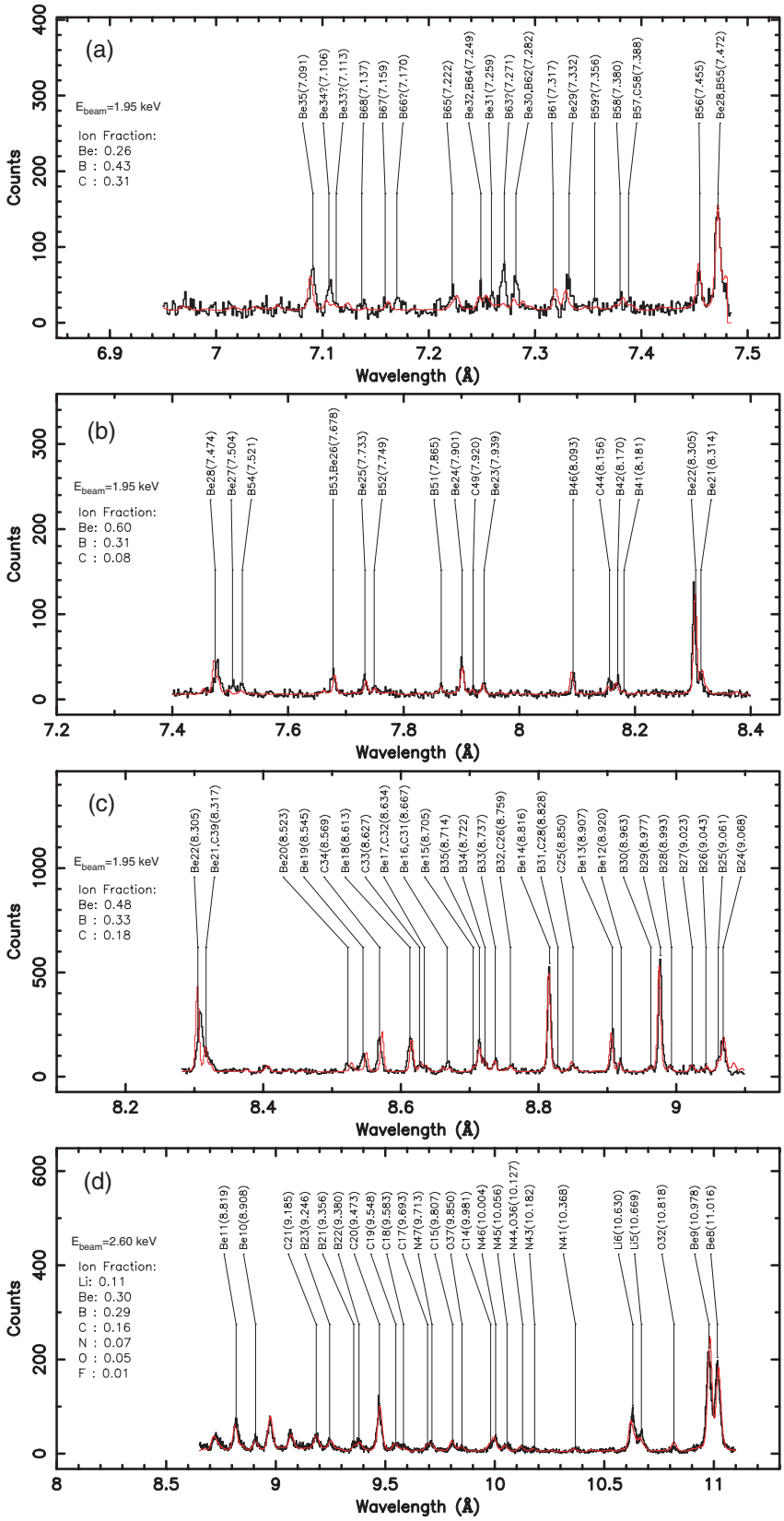

Fig. 6.— Be-like Fe XXIII lines. The black line is the measured data. The red line is the best-fit theoretical model. The electron beam energy of the measurement and the ion charge balance from the model are listed.

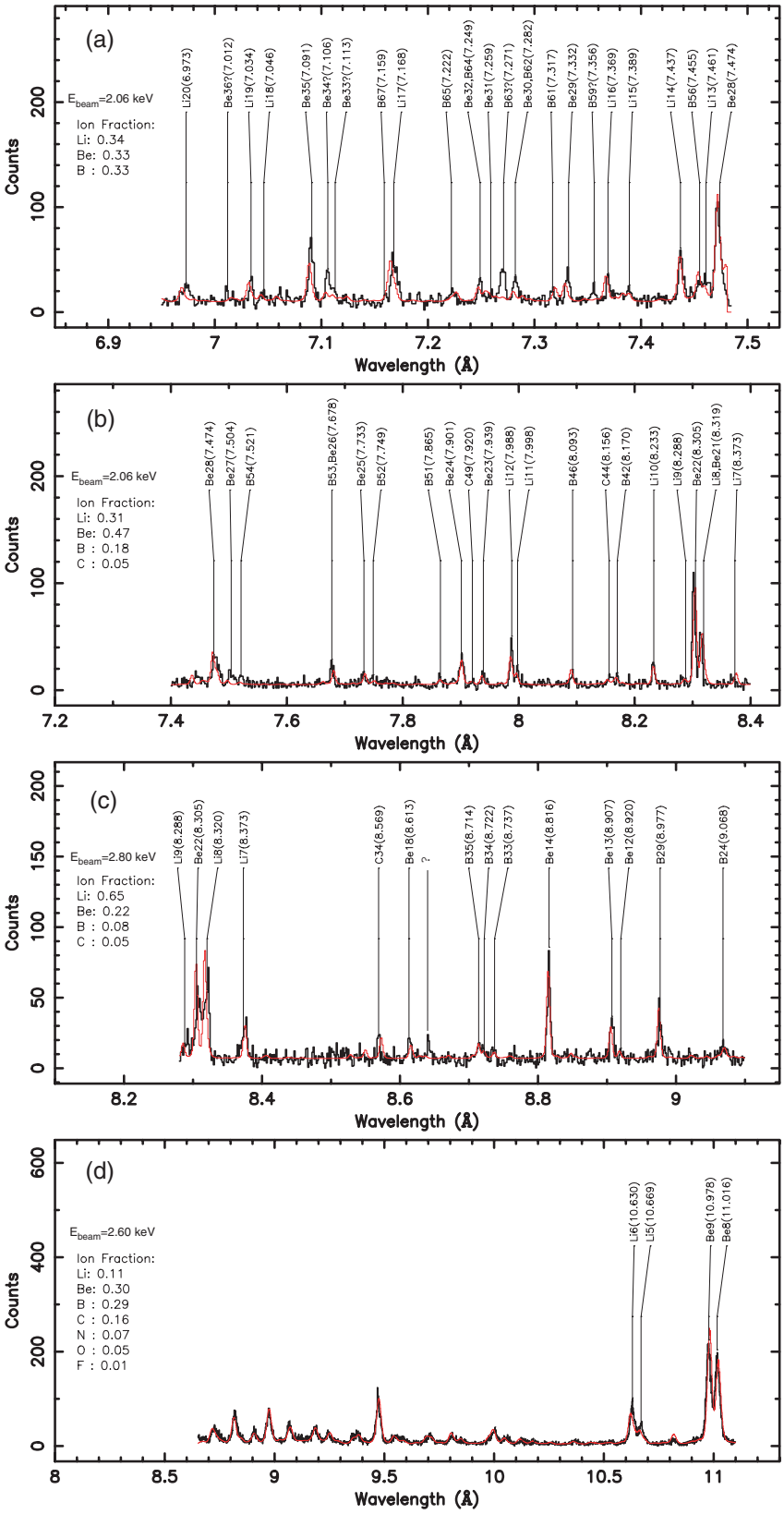

Fig. 7.— Li-like Fe XXIV lines. The black line is the measured data. The red line is the best-fit theoretical model. The electron beam energy of the measurement and the ion charge balance from the model are listed.